ELSEVIER

Polymer 42 (2001) 6631–6639

polymer

www.elsevier.nl/locate/polymer

Structural changes in PNIPAM microgel particles as seen by SANS, DLS, and EM techniques

Karl Kratz[a], Thomas Hellweg[b,1,*], Wolfgang Eimer[a]

[a]Universität Bielefeld, Fakultät für Chemie, Physikalische Chemie 1, D-33615 Bielefeld, Germany
[b]TU Chemnitz, Institut für Physik, Materialforschung und Flüssigkeiten, Reichenhainer Str. 70, D-09107 Chemnitz, Germany

Received 29 February 2000; received in revised form 29 January 2001; accepted 1 February 2001

Abstract

Thermo-sensitive poly(*N*-isopropylacrylamide) (PNIPAM) microgels with different cross-linker density have been investigated by complementary scattering methods and high-resolution imaging techniques. The swelling behavior of the colloidal particles as probed by dynamic light scattering (DLS), is discussed together with information on local structure and dynamics of the particles as obtained from small angle neutron scattering (SANS). Below the volume phase transition the static structure factor reveals liquid-like contributions. This is similar to macroscopic gels, but for low **q** the scattering behavior is different because of the influence of the particle form factor $P(\mathbf{q})$. Beyond the phase transition temperature, T_c, the system becomes completely phase separated and interfacial scattering dominates the measured SANS profiles ($I(\mathbf{q}) \propto \mathbf{q}^{-4}$). Slight deviations from the ideal Porod behavior can be interpreted in terms of surface roughness of the collapsed particles. This corresponds to structures visible on AFM micrographs.

Keywords: Colloidal microgel; Poly(*N*-isopropylacrylamide); Volume phase transition

1. Introduction

Hydro-gels play an important role in living systems and are of broad interest for a large variety of industrial products (e.g. as storage and separation media). They can be regarded as intermediates between solids and liquids, which manifests in a rather complex mixture of the properties of these limiting states. In recent years, especially thermo-sensitive systems like poly(*N*-isopropylacrylamide) (PNIPAM), hydro-gels have attracted much attention [1–3], because the viscoelastic characteristics can be easily controlled by changing the temperature. Moreover, the bio-adhesive properties of these materials point to possible applications as drug delivery systems.

Macroscopic PNIPAM gels have the disadvantage that the swelling/de-swelling process occurs on a rather long time-scale. Fast response to external stimuli, however, is a prerequisite for most potential applications. This problem can be circumvented by decreasing the size of the hydro-gels to mesoscopic dimensions. Therefore, synthesis and characterisation of colloidal microgels has been intensified recently [4,5]. It was found that neutral colloidal PNIPAM particles with a diameter of some hundred nanometres have similar characteristics as their macroscopic counterparts, concerning the transition temperature and swelling capacity of the volume phase transition. Because of their fast kinetic response, microgels are good candidates to gain more insight into the physical nature of the volume phase transition [1,6,7]. For a recent review on microgels, see Ref. [8].

For macroscopic PNIPAM hydro-gels, it is known from dynamic light scattering (DLS) [9] and small-angle neutron scattering (SANS) [3] that the swelling behaviour depends on the amount of cross-linker introduced into the polymer network. Under equilibrium conditions the network elasticity is balanced by the osmotic pressure of the system. The neutron scattering intensity is determined by a solid-like contribution from structural inhomogeneities of the gel matrix and a fluid-like component, which is attributed to local thermal fluctuations of the polymer chains. A growing number of cross-linking points increase the heterogeneity of the network structure. These internal topological constraints reduce the swelling capability of the macroscopic gel.

To characterise the influence of cross-linker density on the volume-phase transition of colloidal PNIPAM hydro-gels, we have studied these systems by complementary scattering methods. DLS provides information about the overall

* Corresponding author. Tel.: +49-30-31422750; fax: +49-30-31426602.
E-mail address: thomas.hellweg@physik.tu-chemnitz.de (T. Hellweg).
[1] Present Address: Iwan-N.-Stranski-Institut, TU Berlin, Strasse des 17 Juni 112, D-10623.

0032-3861/01/$ - see front matter
PII: S0032-3861(01)00099-4

size and shape of the mesoscopic particles [4] in solution and has been used to monitor the temperature-induced swelling/de-swelling process. The internal structure of the microgels has been investigated by SANS. Special emphasis was put on changes in the correlation length for the polymer dynamics across the volume phase transition. In addition, SANS and atomic force microscopy (AFM) have been applied to determine the surface morphology of collapsed microgel particles above the volume phase transition temperature.

2. Theory

We have combined DLS and SANS measurements to obtain complementary information about the overall size (from DLS) and the internal structure (from SANS) of the microgel particles. Due to the large difference in wavelength of the used radiation, different length scales are probed with these methods. For light scattering, $\mathbf{q}R_g \leq 1$, with R_g the radius of gyration and the magnitude of the scattering vector, $\mathbf{q}$, which is given by

$$\mathbf{q} = \frac{4\pi n}{\lambda} \sin\left(\frac{\theta}{2}\right), \tag{1}$$

with n the refractive index of the medium, λ the wavelength of the incident light and θ the scattering angle. In SANS experiments on microgel particles, $\mathbf{q}R_g \gg 1$ is always satisfied. Hence, SANS is a good tool to investigate the internal structure not only of gels [10], but also of colloidal microgel particles.

2.1. SANS

The SANS profiles of swollen macroscopic gels can be described by Ref. [10]

$$I(\mathbf{q}) = I_{\text{liquid}}(\mathbf{q}) + I_{\text{solid}}(\mathbf{q}). \tag{2}$$

$I_{\text{liquid}}(\mathbf{q})$ represents the contribution from concentration fluctuations due to local motion of the polymer chains, which is also observed in a complementary polymer solution [11,12]. For large $\mathbf{q}$, this contribution is best described by a Lorentzian [11]. $I_{\text{solid}}(\mathbf{q})$ is the excess scattering due to the static inhomogeneities introduced into the network by chemical cross-links [3,10,12,13]. Assuming a Gaussian spatial distribution for the cross-links the total structure factor is given by [3]

$$I(\mathbf{q}) = I_G(0)\, exp\left(\frac{-\Lambda^2\mathbf{q}^2}{3}\right) + \frac{I_L(0)}{1+\xi^2\mathbf{q}^2}, \tag{3}$$

where Λ represents a characteristic length scale connected with the static heterogeneities and ξ is the correlation length or blob size [11]. Eq. (3) is a limiting case of a more general form of the structure factor proposed by Horkay and coworkers [13], where the exponent is allowed to differ from 2 if the spatial distribution of the heterogeneities is not Gaussian. For the correlation length the following scaling law

$$\xi \propto \left|\frac{T - T_c}{T_c}\right|^{-\nu} \tag{4}$$

should hold (with $\nu = 0.65$ for gels) [3]. T_c is the volume phase transition temperature.

In our experiments, we are looking at spherical colloidal particles and in this case the particle form factor, $P(\mathbf{q})$, cannot be neglected [14]. However, for particles with $R_G \gg \mathbf{q}^{-1}$ only the Porod region of $P(\mathbf{q})$ should contribute significantly to the scattering intensity. In the Porod region, the scattering arises from the particle surface and the data should be well described by expressions of the type

$$I(\mathbf{q}) = \frac{A}{V}\frac{1}{\mathbf{q}^4} + \frac{I(0)_L}{1+\xi^2\mathbf{q}^2}. \tag{5}$$

In this equation, A is the interfacial area in the scattering volume and V is the scattering volume. Similar phenomenological descriptions of microgels were already used before [14]. The contribution from the cross-links is omitted in this description. Beyond the transition temperature, we are dealing with a phase-separated system and the scattering arises from the interface between the collapsed polymer particle and the surrounding solvent. For flat interfaces, the structure factor is given by Porod's law

$$I(\mathbf{q}) \propto \mathbf{q}^{-4}. \tag{6}$$

2.2. DLS

DLS monitors fluctuations in the scattered electrical field by means of the field time autocorrelation function given by

$$g^1(t) = \exp(-\Gamma t) \tag{7}$$

for monodisperse systems and provides therefore knowledge about the translational motion of the scattering particles in the sample [15]. The characteristic relaxation rate Γ is given by

$$\Gamma = D\mathbf{q}^2, \tag{8}$$

with D the mutual translational diffusion coefficient. Real colloidal systems always are more or less polydisperse and in this case the field time autocorrelation function is given by a weighted sum of exponentials

$$g^1(t) = \int G(\Gamma)\, exp(-\Gamma t)\, d\Gamma. \tag{9}$$

$G(\Gamma)$ is the relaxation rate distribution representing the contribution from the different particle sizes. To compute the mean value and the broadness of this distribution function, the measured correlation functions can be analyzed using the method of cumulants [16] or by means of an inverse Laplace transform [17,18]. For the second method, several different software packages are available and in the present study we used the FORTRAN program CONTIN provided by

S. Provencher [17,18]. Both methods provide a z-averaged $\langle \Gamma \rangle$ and, therefore, a z-averaged translational diffusion coefficient.

$$\langle D \rangle = \frac{kT}{6\pi\eta R_h}. \quad (10)$$

Here, T is the temperature, k the Boltzmann constant, η the viscosity of the solvent, and R_h is the radius of a hydrodynamically equivalent sphere. For an ideal dilute solution of non-interacting particles D corresponds to the self-diffusion coefficient. For more details, see for example Refs. [15,19].

3. Experimental

3.1. Sample preparation

Synthesis of the PNIPAM particles and sample preparation for the light scattering experiments has been described in Ref. [4]. For the neutron scattering experiments, a fraction of the microgel particles was dried at a temperature of 313 K. Afterwards the particles were dissolved in D_2O (99.8% isotopic purity; Eurisotop, Groupe CEA — Saclay). It is known that for D_2O the phase transition temperature of PNIPAM can be slightly different [3], therefore, we have checked the influence of D_2O on the phase transition temperature by DLS for a sample containing 7.33% cross-linker (BIS). We found the phase transition temperature shifted by 0.8 K to higher temperatures for the D_2O solutions. This is in good agreement with results found by Shibayama et al. for macroscopic PNIPAM gels [3]. The parameters describing the different samples are listed in Table 1.

3.2. DLS

The light scattering experiments were performed using a classical goniometer set-up (ALV Langen) and an argon ion laser (Coherent Innova 90) operating in single mode at a wavelength of 488 nm. The single mode output was obtained by placing a thermostated etalon into the laser resonator. The samples were positioned in an index matching bath (toluene), which was thermostated with a temperature stability of ± 0.1 K. The scattering geometry was defined to be VV using a Glan polariser for the incident beam and a Glan–Thompson polariser in front of the photo-multiplier (PM) employed for the detection of the scattered light. The fluctuations of the scattered intensity were analysed with an ALV-5000 digital correlator. For additional descriptions of the experimental set-up see Ref. [20].

Table 1
Characteristics of the investigated PNIPAM microgels. The volume phase transition temperatures, T_c, were determined in dilute aqueous solution by monitoring the hydrodynamic radii R_h using DLS. In D_2O, the values are found to be ≈ 0.8°C higher. The de-swelling curves obtained in this way are also the basis for the calculation of the de-swelling ratio α (see Eq. (11)). The given values of the hydrodynamic radii R_h are those found for the swollen state at $T = 15$°C. The error for these values is, approximately, 5%. Additionally, the radii R_{SEM} obtained from the analysis of the electron micrographs are given. These are lower because they were obtained for dried particles

Cross-linker (mol%)	R_{SEM} (nm)	R_h (nm)	T_c (°C)	α
0.73	221 ± 15	298	31.3	0.032
1.47	212 ± 18	286	31.8	0.110
3.67	222 ± 14	304	31.6	0.084
7.33	202 ± 10	277	31.4	0.144
11	314 ± 12	350	32.7	0.273

3.3. SANS

The SANS experiments presented here, were carried out at the 'Forschungszentrum Jülich' and in part at the 'Laboratoire Léon Brillouin — Laboratoire Commun CEA–CNRS' using the KWS1 machine and the PAXY machine, respectively. For details of both set-ups, see the relevant publications of both institutes.

The data were collected in both cases using two-dimensional multidetectors. These data have been corrected for the efficiency of the different detector cells using a water spectrum and then because of the isotropic character of the scattering, they were circularly averaged. After correction for the scattering of the solvent and the empty cell, the data were brought on an absolute scale. For the Jülich data, the spectrum of a Lupolen standard was used for the calibration of our experimental data [21]. After calibration, data obtained for different sample to detector distances overlapped within the experimental error interval and no further adjustment was necessary. Calibration of the Saclay data was done using the method described in Ref. [22]. This calibration is based on the determination of an attenuation factor of the primary beam intensity. The details are not presented, because the absolute intensities are not discussed in this study.

3.4. SEM and AFM

Electron micrographs have been taken from microgel particles fixed on commercially available microscope slides covered with poly-L-lysine (Sigma — Aldrich). After removing of surplus amounts of solution, the samples were washed three times with distilled water and successively dried at room temperature for about 24 h. Then the glass supports were positioned on an aluminium plate and afterwards covered with a gold layer using a Hummer VII sputtering system. For the electron micrographs, we employed a Hitachi S450 microscope. The sample holder was tilted by 30° to increase the contrast of the samples.

The same samples have been investigated using a OMICRON AFM/STM, which allows to obtain a better spatial resolution then SEM.

4. Results and discussion

4.1. Overall size and shape of the microgel particles

PNIPAM microgels with different cross-linker density have been prepared by surfactant-free emulsion polymerisation [4]. The hydrodynamic radius of the colloidal particles in the swollen state at low temperature ranges from 270 to 350 nm as determined by DLS measurements (see Table 1). The size of the microgels depends on the individual preparation conditions [4].

In Fig. 1A and B typical distributions of relaxation rates from a CONTIN analysis of the intensity auto-correlation function are displayed for two significantly different cross-linker densities. In both cases, a single narrow distribution of relaxation rates is obtained by Laplace inversion of the experimental correlation functions. These peaks can be attributed to translational diffusion and manifest the almost monodisperse size distribution of the colloidal particles. Their hydrodynamic dimensions were calculated from the

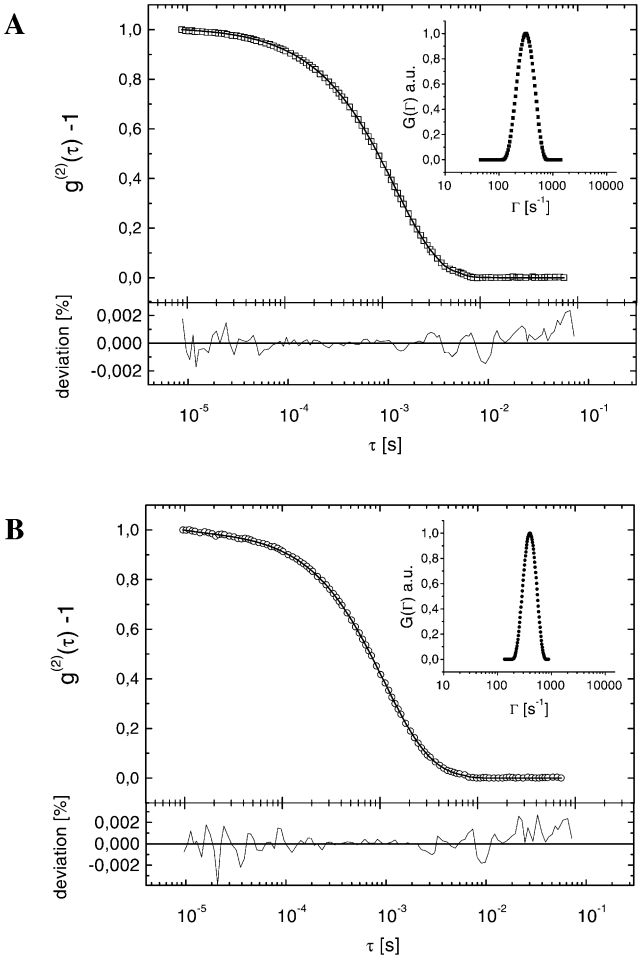

Fig. 1. (A) Example for the DLS results obtained for low cross-linker concentration (0.73% BIS). (B) Example for the DLS results obtained for high cross-linker concentration (7.33% BIS). The insets show the obtained distribution of relaxation rates as computed by a CONTIN analysis. In both cases, the polymer concentration was 0.05 μg/ml.

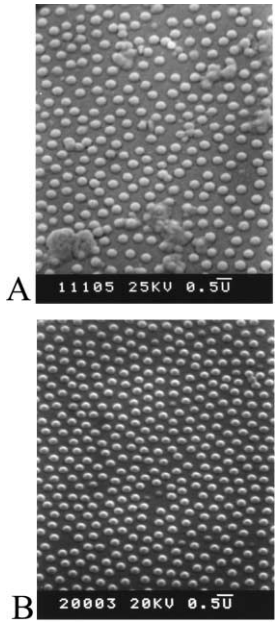

Fig. 2. SEM micrographs of PNIPAM with different cross-linker concentration. (A): 0.73%; (B): 7.33%.

z-averaged diffusion coefficient according to the Stokes–Einstein equation. Radii of the different samples are summarised in Table 1.

The same samples have been investigated by SEM which provides complementary information about the shape of the microgel particles. Typical micrographs are presented in Fig. 2A and B. All dried microgels reveal a spherical shape and the ordered structure on the supporting surface demonstrates their high monodispersity. This is in good agreement with the DLS results.

4.2. Swelling behaviour of the microgels

The collapse of the colloidal microgel particles across the volume phase transition has been followed by DLS. The change in hydrodynamic radius, R_h, was determined within a temperature range from $T = 15$ to 45°C. To characterise the swelling capacity for different cross-linker densities, we have calculated the de-swelling ratio α according to

$$\alpha = \left(\frac{R_h}{R_h^0}\right)^3 = \left(\frac{V}{V_0}\right). \tag{11}$$

For the reference radius, R_h^0, we have chosen the value obtained at $T = 1.5$°C, where the gels are swollen to their maximum size. As shown in Fig. 3, the shrinking of the microgels proceeds nearly discontinuously for microgels with a cross-linker content below 2%. For highly cross-linked microgels ([BIS] $\geq$ 5%), the transition range broadens significantly. Compared to other studies of the swelling behaviour [23] our particles behave slightly different. In the region between 10 and 22.5°C no significant decrease of the hydrodynamic radius occurs (within the experimental error of $\approx$ 5%). For a 2% BIS containing microgel sample, Senff

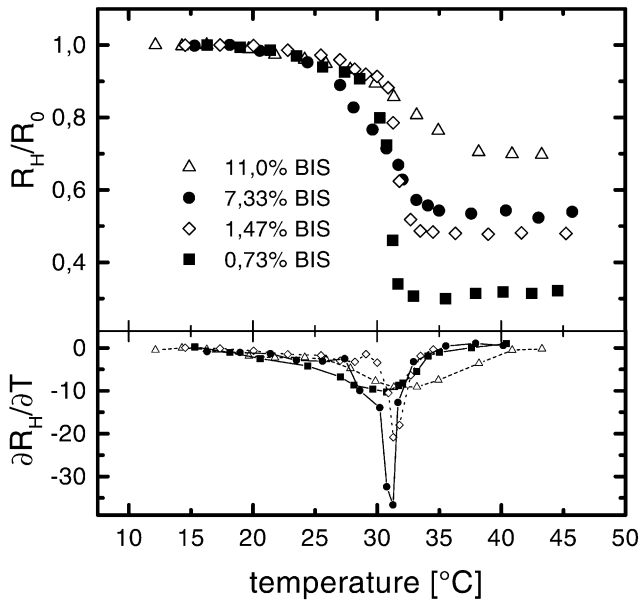

Fig. 3. Hydrodynamic radii for several different microgels as a function of temperature. Additionally the derivatives, $(\partial R/\partial T)$, of these swelling curves are shown. The derivatives are used to determine the points of inflection of the swelling curves, which are given as the phase transition temperature for the respective microgel (from △: 11.0% BIS to ●: 0.73% BIS). It can be seen that due to the broadening of the decrease in R_h for [BIS] ≥ 5% the resulting phase transition temperature is less precise.

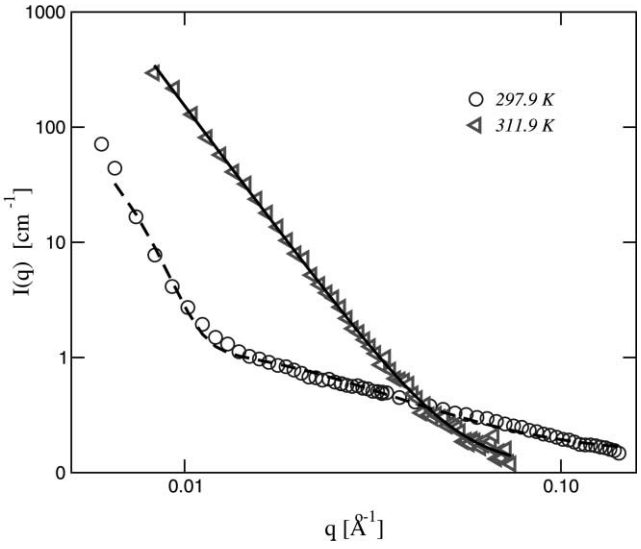

Fig. 4. SANS profiles for low and for high temperature. The shown data were obtained for a sample containing 7.33% BIS. The dashed line represents a fit to Eq. (3). The scattering curve from the shrunken particles is fitted to expressions of the type $I(\mathbf{q}) \propto (1/\mathbf{q}^{\alpha})$ with $\alpha \approx 4.2$ (solid line).

and coworkers found a constant decrease of R_h [23]. This difference in behaviour might be due to the difference in preparation (lower starter concentration), which leads to a lower surface charge density for our particles.

As expected from previous experiments [4], we observed that the swelling ratio decreases with increasing amount of BIS (see Table 1), which can be attributed to topological constraints that are introduced into the polymer network through an increasing number of cross-linking points. The transition temperature, however, remains almost constant, indicating that the thermodynamics (interaction between the PNIPAM chains and the solvent) that determine the de-swelling process were not changed significantly.

Having characterised the overall size and shape of the colloidal microgel particles, we now turn to their internal structure which can be explored by SANS.

4.3. Internal structure of the microgels

We have investigated the morphology of the colloidal PNIPAM microgel particles with different cross-linker density by SANS. Temperature-dependent measurements provide information about structural changes across the volume phase transition. Typical examples for spectra below and above the transition temperature are presented in Fig. 4. Similar scattering curves for slightly different microgels were already observed before [5,14]. The scattering profiles of the microgels in the swollen and the collapsed state decrease monotonically with increasing wave vector. In the swollen state, we can expect that dynamic concentration fluctuations as well as permanent departures from uniformity due to the cross-links contribute to the scattering intensity. This behaviour is already known from

Table 2
Summary of the SANS results found below the phase transition temperature. The values in brakets were calculated for a sample very close to the collapse

T (°C)	0.73% BIS		1.47% BIS		3.67% BIS		7.33% BIS	
	$I_L(0)$ (cm^{-1})	ξ (Å)	$I_L(0)$ (cm^{-1})	ξ (Å)	$I_L(0)$ (cm^{-1})	ξ (Å)	$I_L(0)$ (cm^{-1})	ξ (Å)
5.19	–	–	0.02	21	0.57	27	0.36	20
15.9	–	–	0.28	36	0.78	32	0.41	23
22.9	–	–	0.48	44	0.86	30	0.59	24
24.8	1.9	32	0.39	34	0.93	29	0.82	24
26.7	–	–	0.74	48	1.06	30	0.89	25
29.5	–	–	0.67	43	1.08	30	0.89	25
29.6	(80)	(223)	1.29	53	1.39	32	1.24	29
30.5	–	–	–	–	2.13	41	1.93	40
31.4	–	–	–	–	–	–	1.65	39

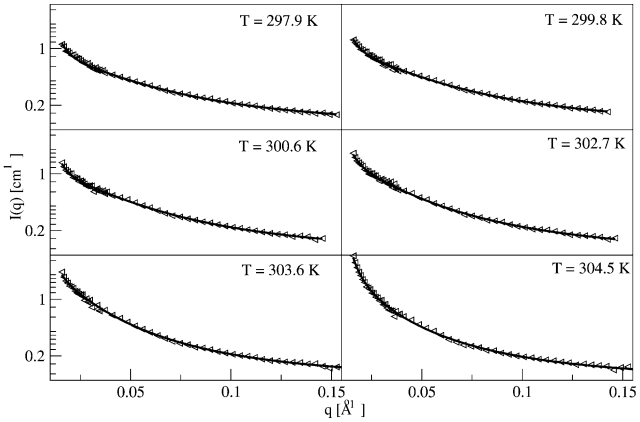

Fig. 5. Example for a temperature dependent series of SANS measurements. Shown data were obtained for a 7.33% BIS containing sample. The solid lines indicate fits to Eq. (5).

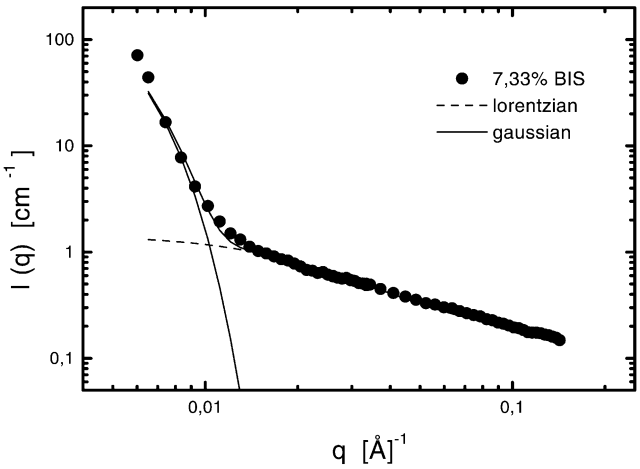

Fig. 7. The experimental data shown were measured for a sample prepared with a cross-linker content of 7.33% at a temperature of 298.8 K. The lines representing the two contributions have been calculated from results of the fit to Eq. (3). The fit does not lead to satisfying results. At low **q**, strong deviations occur and for higher **q**-values the curvature of the Lorentzian does not satisfyingly follow the curvature of the experimental data (see also Fig. 8). This is due to the fact that the particle form factor still dominates the scattering. Also the other curves show a similar behavior.

macroscopic gels. For microgel particles additionally the form factor, $P(\mathbf{q})$, may contribute to the small angle scattering. The shrinking of the microgel particles beyond the transition temperature leads to a change in scattering contrast arising from an almost complete expulsion of the solvent. The resulting SANS profiles are dominated by scattering from the interfaces between the colloidal particles and the surrounding solvent. Because of the characteristic differences in the scattering behaviour, we will discuss the two temperature regimes, below and above the volume phase transition, separately.

4.3.1. Scattering behaviour in the swollen state, $T < T_c$

The scattering profiles for all cross-linker densities and temperatures were fitted by Eq. (3) and by Eq. (5). We did not obtain satisfying results using Eq. (3). At low **q**, the increase of the scattering curves is stronger then predicted by the model and for large **q**, the curvature of the data differs from the fit especially for the higher cross-linker concentrations. Therefore, in Table 2 only the results from the fit using Eq. (5) are given. In Fig. 5, the scattering profiles measured for the 7.33% BIS cross-linked samples are shown together with the respective fits to Eq. (5).

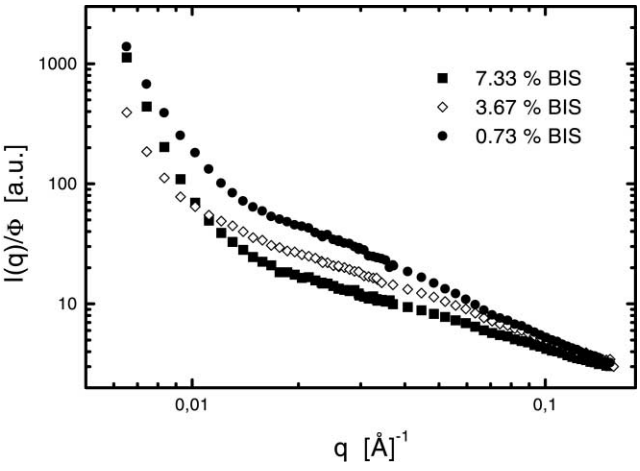

Fig. 6. Experimental results for three different cross-linker concentrations. The SANS profiles are normalised with respect to the polymer volume fraction, ϕ. For the lowest cross-linker concentration the highest contribution of $I_{\text{liquid}}(\mathbf{q})$ can be observed.

In general, we observe that the contribution from the particle form factor $P(\mathbf{q})$ dominates the scattering intensity at low **q**. Fig. 6 shows examples of scattering profiles as obtained for three different cross-linker concentrations. It can be seen that for the lowest cross-linker concentration (0.73% BIS) the liquid-like contribution is more important than for the higher concentrations. In Fig. 7, a detailed example for the fit of the low temperature data to Eq. (3) is shown. The individual Gaussian and the Lorentzian contribution are calculated from the results of the non-linear fit to Eq. (3). The representation of the high **q** data by the Lorentzian is satisfactory, whereas the low **q** part of the spectra showed deviations from the Gaussian form. Therefore, we have also computed the fit to structure factors based on the more general model of Horkay and coworkers [13], varying the stretching exponent in Eq. (3) between 0.7 and 2 (results not shown). However, this did not lead to improvements in terms of χ^2 of the fit compared to the simple Gaussian form.

In Fig. 8, a comparison of fits to Eqs. (3) and (5) is given. At low **q**, the scattering profile is better described by the $\mathbf{q}^{-4}$-dependence of Eq. (5). This leads also to a better fit at high **q** and therefore to more reliable results for ξ. From the decrease of the correlation length (see Table 1), we conclude that the polymer network becomes more heterogeneous with increasing cross-linker density, which has also been observed for other macroscopic gels [24–26]. Moreover, the correlation length of the blobs, ξ, reveals the same

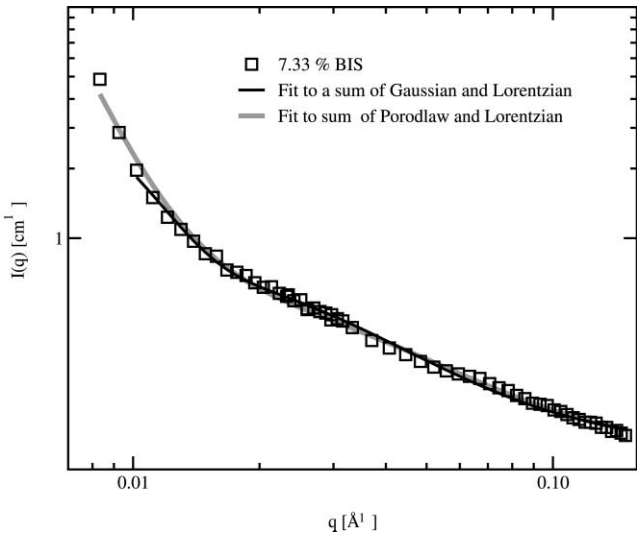

Fig. 8. Comparison of fits to Eq. (3) and Eq. (5). It is obvious that the increase at low **q** is better described by the $\mathbf{q}^{-4}$-dependence in Eq. (5).

size range for the macroscopic and microscopic gel systems. For example, for a 4.5 mol% BIS containing PNIPAM microgel similar values were presented [14]. One may conclude that the very local conformation of the polymer chain is not significantly affected by the preparation conditions. It is however, worth mentioning that the measurements of macroscopic gels have been done under isochoric conditions and only a few samples could attain swelling equilibrium [3].

4.3.2. Scattering behavior of the collapsed particles, $T > T_c$

Above the volume phase transition of the polymer, the scattering behaviour of the microgel particles changes dramatically compared with that at a lower temperature. Moreover, the SANS profiles are different from those observed for macroscopic gels [2,3]. This is due to the fact that there exist no long range mechanical constraints as in macroscopic gels and therefore the microgel particles are able to collapse completely. A Debye–Bueche form, which was proposed as a structure factor for collapsed macroscopic gels [2] does not describe the scattering curves of the microgel particles beyond the phase transition temperature.

A first estimate points to simple interfacial scattering ($I(\mathbf{q}) \propto \mathbf{q}^{-4}$) [27], but a linear fit to a log–log plot of the data revealed a slope, which differs slightly from -4. Moreover, we have investigated the collapsed microgel particles by AFM and found evidence for a grain structured surface as shown in Fig. 9. The surface structure of the particles shows a 'raspberry' like pattern. Because we used the same samples to obtain SEM and AFM micrographs, small gold cluster (10 nm) are visible on the AFM images.

4.3.3. Surface roughness of collapsed PNIPAM microgels

AFM micrographs suggest that the SANS scattering profiles observed for the collapsed microgels arise from a

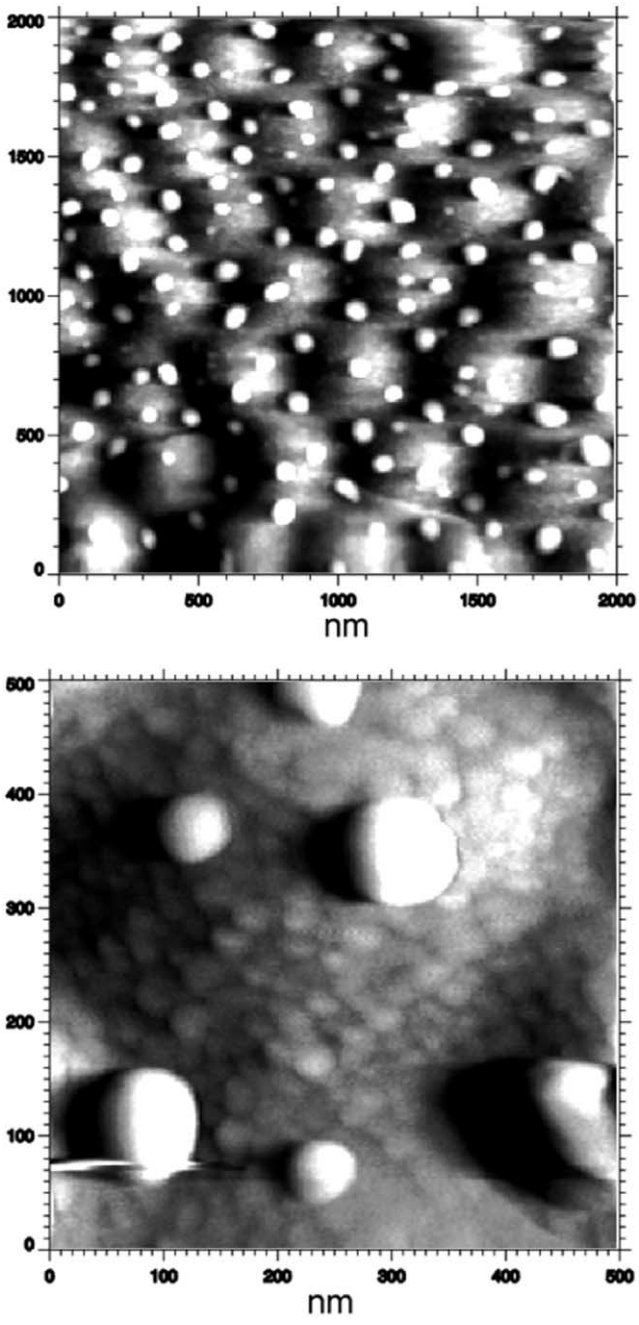

Fig. 9. AFM images of microgel particles with 5.87% cross-linker content (BIS). Samples are sputtered with gold.

certain roughness of the particle interface. For rough surfaces, the interfacial area depends on the scale of observation [27]. An approach accounting for this effect has been published by Bale and coworkers [28]. They describe the scattering curves by $I(\mathbf{q}) \propto 1/\mathbf{q}^{\alpha}$ with $3 < \alpha < 4$. This description of the scattering profiles often was applied to microporous systems. The scattering profiles of the collapsed microgels can be fitted by the same relation, but we always get $\alpha > 4$. In Fig. 10, data for samples prepared with three different cross-linker concentrations

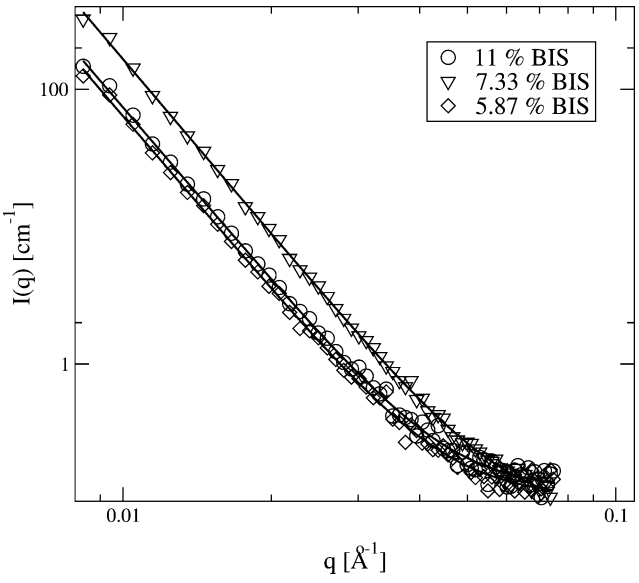

Fig. 10. High temperature data for three different cross-linker concentrations. The lines correspond to a fit according to $I(\mathbf{q}) \propto (1/\mathbf{q}^{\alpha})$. In all cases, the exponent is found to be $\approx 4.25 \pm 0.05$. This can be interpreted in terms of the approach of Wong [29]. The measurements presented here have been done at the LLB.

are shown. The curves have been measured at a temperature $T = 312.3$ K.

In the fit, an additional baseline component is used to account for the incoherent background scattering. The baseline was not adjusted but set to the value of I($\mathbf{q}$) measured at the largest $\mathbf{q}$.

However, the system investigated here has a different lengthscale–reciprocal scattering vector relationship and a narrow length distribution. Therefore, here a more complete theoretical model considering the surface roughness in small-angle neutron scattering developed by Wong [29] may apply. In this model, scattering exponents, α, larger than 4 are predicted for surface fractals and the simple $\mathbf{q}^{-4}$-dependence of the scattered intensity in the Porod regime is modified by an additional contribution (see Eq. (12))

$$I(\mathbf{q}) \propto \frac{a}{\mathbf{q}^{3+x}} + \frac{b}{\mathbf{q}^{4}}. \tag{12}$$

Here, x is a parameter which contains the roughness of the scattering interface [20]. Fits to Eq. (12) lead to a satisfying representation of the SANS profiles. This is no contradiction to Bale's approach, but just due to different validity intervals of the two descriptions. From the fit, we get a value for x which is 1.3 for all SANS profiles shown here, but due to the increased number of parameters the error for x is higher than the error for α. Because $x > 1$, according to the theoretical model [29], the surface of the microgel particles qualifies as a fractal with a Hausdorff dimension [30] of $D = 1 + x = 2.3$. The constant scaling parameter x for the different samples indicates that the surface roughness does not depend on the amount of cross-linker molecules introduced into the polymer network. But however, due to the limited precision of the experimental data the absolute value of x, obtained from the fit might have a large error. From the fitting procedure we obtain a mean relative error of $\pm 10\%$. The error for α is $\leq 5\%$.

A possible explanation for the surface roughness might be the formation of dangling polymer chains during the synthesis. Such chains on the surface would lead to an entropic stabilisation of the microgel solutions and when they collapse a surface pattern like in Fig. 9 will be obtained.

5. Conclusions

The small-angle neutron scattering profiles of PNIPAM microgel particles in heavy water solution depend dramatically on the temperature. In the swollen state, thermal density fluctuations, due to the dynamics of the polymer network contribute to the scattered intensity. The characteristic blob size, ξ, seems to decrease with increasing cross-linker density and compares well with the respective lengths determined for macroscopic PNIPAM hydrogels and for other microgels.

However, it is not possible to apply the same models to microgels as were used for macrogels. This is due to the fact that the Porod region of the particle form factor (scattering from the particle interfaces, $I(\mathbf{q}) \propto \mathbf{q}^{-4}$) is not completely decayed in the low $\mathbf{q}$-interval of the measurements. Therefore, the fit to Eq. (3) is perturbed and the solid-like contribution found for macroscopic gels (for macroscopic gels no form factor contribution has to be taken into account) cannot be resolved in this study. From the data presented here, it was not possible to check whether the correlation length ξ scales like predicted for gels when approaching the volume phase transition temperature. This is due to the rather high uncertainty in the determination of the phase transition temperature. In future studies, it might be possible to address this point again, when the precision of the determination of the critical temperature can be improved and a better statistics of the scattering curves may lead to a higher precision in the determination of ξ.

Above the volume phase transition point, the PNIPAM particles collapse completely and the resulting scattering pattern shows Porod behaviour in first approximation. The internal dynamics is completely frozen (the Lorentzian contribution disappeared from scattering curves). A more detailed analysis of these SANS profiles allows for the determination of the surface roughness of the collapsed particles applying the Wong description of interfacial scattering. This roughness also manifests in the raspberry-like pattern seen on AFM micrographs of collapsed particles and which may arise from the collapse of dangling polymer chains on the particle surface. Moreover, the fit to Eq. (12) provides evidence for a fractal surface structure with a Hausdorff dimension $D = 2.3 \pm 0.1$ for the collapsed particles.

Acknowledgements

The authors would like to thank W. Pyckhout–Hintzen and E. Dubois for help with the respective small angle machines. We are grateful to A. Brûlet and F. Boué for fruitful discussions. Moreover, we would like to thank J. Hartwig and M. Sundermann for performing the AFM-measurements. This project was supported by the Deutsche Forschungsgemeinschaft.

References

[1] Hirokawa Y, Tanaka T. J Chem Phys 1984;81:6379.
[2] Shibayama M. Macromol Chem Phys 1998;199:1.
[3] Shibayama M, Tanaka T, Han CC. J Chem Phys 1992;97:6829.
[4] Kratz M, Eimer W. Ber Bunsenges Phys Chem 1998;102:848.
[5] Kratz K, Hellweg T, Eimer W. Ber Bunsenges Phys Chem 1998;102:1603.
[6] Oh KS, Oh JS, Choi HS, Bae YC. Macromolecules 1998;31:7328.
[7] Dingenouts N, Nordhausen C, Ballauff M. Ber Bunsenges Phys Chem 1998;102:1594.
[8] Pelton R. Adv Colloid Interf Sci 2000;85:1.
[9] Matsuo ES, Tanaka T. J Chem Phys 1988;89:1695.
[10] Hecht A-M, Duplessix R, Geissler E. Macromolecules 1985;18:2167.
[11] De Gennes P-G. Scaling concepts in polymer physics. Ithaca and London: Cornell University Press, 1979.
[12] Mallam S, Horkay F, Hecht A-M, Rennie AR, Geissler E. Macromolecules 1991;24:543.
[13] Horkay F, Hecht A-R, Mallam S, Geissler E, Rennie AR. Macromolecules 1991;24:2896.
[14] Crowther HM, Saunders BR, Mears SJ, Cosgrove T, Vincent B, King SM, Yu G-E. Coll Surf A 1999;152:327.
[15] Berne BJ, Pecora R. Dynamic light scattering. New York: Wiley, 1976.
[16] Koppel DE. J Chem Phys 1972;57:4814.
[17] Provencher SW. Comp Phys Com 1982;27:213.
[18] Provencher SW. Comp Phys Com 1982;27:229.
[19] Hellweg T, Eimer W. Coll Surf A 1998;136:97.
[20] Patkowski A, Seils J, Hinssen H, Dorfmüller T. Biopolymers 1990;30:427.
[21] Poppe A, Willner L, Allgaier J, Stellbrink J, Richter D. Macromolecules 1997;30:7462.
[22] Cotton JP. Initial data treatment. In: Linder P, Zemb T, editors. Neutron, X-ray and light scattering. Amsterdam: Elsevier, 1991.
[23] Senff H, Richtering W. J Chem Phys 1999;111:1705.
[24] Mallam S, Horkay F, Hecht AM, Geissler E. Macromolecules 1989;22:3356.
[25] Schoessler F, Skouri R, Munch JP, Gandau JS. J Phys II 1994;4:1221.
[26] Shibabyama M, Norisuye S. Macromolecules 1996;29:8746.
[27] Auvray L, Auroy P. Scattering by interfaces: variations on Porod's law. In: Lindner P, Zemb T, editors. Neutron, X-ray and light scattering. Amsterdam: Elsevier, 1991. p. 199–221.
[28] Bale HD, Schmidt PW. Phys Rev Lett 1984;53:596.
[29] Wong P. Phys Rev B 1985;32:7417.
[30] Mandelbrot BB. The fractal geometry of nature. 2nd ed. New York: Freeman, 1983.